ELSEVIER

Surface and Coatings Technology 149 (2002) 198–205

SURFACE & COATINGS TECHNOLOGY

www.elsevier.com/locate/surfcoat

Computed depth profile method of X-ray diffraction and its application to Ni/Pd films

Huaqiang Wu, Bin Li, Wei Miao, Xingtao Liu, Kun Tao*

Department of Materials Science and Engineering, Tsinghua University, Beijing 100084, PR China

Received 23 April 2001; accepted in revised form 30 July 2001

Abstract

This paper develops a method that uses parallel beam X-ray diffraction (XRD) for profiling structure and phase distributions along with the depth. This method was used to characterize the Ni/Pd thin film sample and to obtain the phase depth profile. In the data analysis procession, the non-negative least square (NNLS) algorithm was introduced to resolve the ill-posed inverse problem that emerged in the solving procession. The grains with same crystallographic orientation were measured when the incident angles varied in the designed diffraction manner and the influence of the texture in the films was avoided properly. It should be noticed that this method is employed for the first time to analyze a system containing more than two phases.

PACS: 61.10.Wg; 68.55.Nq; 68.65.+g

Keywords: X-Ray diffraction; Ni/Pd thin film; Depth profiling

1. Introduction

Recently, the analysis of thin films and surface layers has become an interesting field of materials studies [1,2]. The X-ray diffraction (XRD) analysis, which is a non-destructive method and does not require specific sample preparation, has been widely used to identify the phase and structure variations of samples. To obtain phase depth profiles, the concept of information depth or penetration depth [3–5] has been used to define the specific depth semi-quantitatively, where the corresponding diffraction information is concerned. In other works [6–9], the concept of absorption depth was employed when trying to obtain the structure depth profiling quantitatively. The method is similar to a special kind of computed topography (CT), and was named as the computed depth profiling (CDP) method of XRD patterns.

The purpose of this paper is to present the development of the CDP method in mathematical algorithms and application range. This time the CDP method was used to analyze a system with three phases. The Ni/Pd film annealed at 380°C for 30 min was analyzed by this method. With the operation of the Bruker D8 Discover diffractometer, samples can be rotated around three independent axes ensuring that the grains with the same crystallographic orientation participate in the diffraction process while the incident angle varies. At the same time, the experimental data has improved mechanical precision that compared with previous work. Rutherford Back Scattering (RBS) experiments were performed to obtain elemental depth profiles.

2. Theory

2.1. Main assumptions

The objects that the CDP method studied are either thin films or surface layers of bulk materials. According

* Corresponding author. Fax: +86-10-6277-1444.
E-mail address: taokun@mail.tsinghua.edu.cn (K. Tao).

PII: S0257-8972(01)01442-6

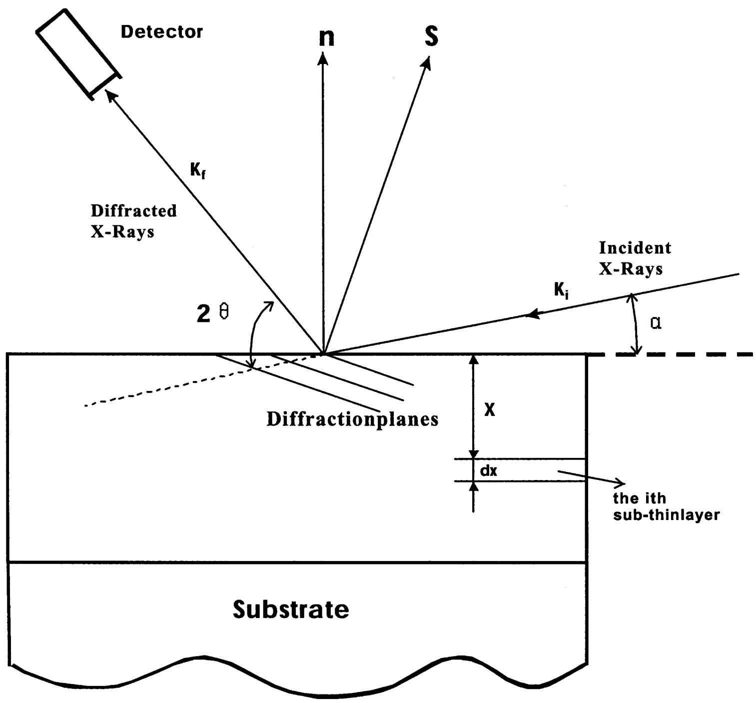

Fig. 1. The asymmetrical Bragg diffraction scheme.

to our previous work [6–9] and the work of Bolle et al. [10], the main assumptions in the CDP method are as follows: (i) the phase distribution and their structures in the sample vary with the depth, but are homogeneous in the direction parallel to the surface at any depth; (ii) crystallographic texture is homogeneous in the film, i.e. no texture gradient present; (iii) the concentration increases or decreases continuously and monotonically in the film from its outside to inside; (iv) the size of each analyzed sub-layer should be greater than the length of the X-ray coherent domain; (v) the whole thickness of the layer analyzed is penetrated by the X-rays' beam.

2.2. Physical model

In the experiments, the asymmetrical diffraction method, as shown in Fig. 1, was used to measure the diffraction patterns with different incident angles α. Vector n is the normal to the sample surface and s is the diffraction vector. In our measurements, the sample was rotated around the axis s and the variation of the rotation angle corresponded to the variation of the incident angle α. Consequently, in the present experimental scheme, the grains with the same crystallographic orientation were measured at each incident angle.

As shown in previous work [6,8], as a function of orientation, the XRD experimental intensity can be expressed by:

$$I_{\text{obs}}(\alpha,\theta,\bar{s}) = A(\alpha,\theta,\bar{s})\cdot\int_0^\infty I(x,\theta,\bar{s})\cdot\exp(-\sigma Y)dx \quad (1)$$

Here,

$$Y = Y(x) = \int_0^x \mu(x)dx \quad (2)$$

$$\sigma = \sigma(\alpha,\theta,\bar{s}) = 1/\sin\alpha + 1/\sin\beta \quad (3)$$

where $I_{\text{obs}}(\alpha,\theta,\bar{s})$ is the measured X-ray diffraction intensity; the $I(x,\theta,\bar{s})$ represents the diffraction information of the infinitesimal sub-thin layers at depth x in the diffraction angle θ with the orientation s. The concept of diffraction ability $I(x,\theta,\bar{s})$ includes the influences of structure and the volume percentage of phases, but excludes the influence of the experimental conditions and geometrical factors. The $\mu(x)$ is the linear absorption coefficient of the sub-thin layer at depth x; β is the angle between the diffraction beam and sample surface; σ is the diffraction geometrical factor; the $Y(x)$, which is defined as the absorption depth, can be used to linearize the non-linear items in the following calculation and can also be regarded as a depth scale directly; and $A(\alpha,\theta,\bar{s})$, which takes into account the influence of the diffraction geometry as well as the size and shape of the sample, can be obtained by the measurement of a standard sample with uniformly arbitrary phase and with the identical size and shape to the sample and-under the same diffraction geometry.

Let $I^*_{obs}(\sigma)=I_{obs}(\alpha,\theta,\vec{S})/A(\alpha,\theta,\vec{S})$
$I^*(Y)=I(Y(x),\theta,\vec{s})/\mu(x)$

$$\text{So } I^*_{obs}(\sigma)=\int_0^D I^*(Y)\cdot\exp(-\sigma Y)dY \tag{4}$$

where D is the total thickness of the thin film in terms of absorption depth Y scale. If the substrate matter contributes very little to the experimental diffraction intensity, D should be used in Eq. (4) instead of infinite thickness.

2.3. Mathematical method

The resolving procession was a typical ill-posed inverse problem in mathematics. The constrained linear inversion method has been used to obtain $I^*(Y)$ in Eq. (4). However, because the $I^*(Y)$ should actually be non-negative, the algorithm non-negative least squares (NNLS) is employed to meet this constraint and is combined with constrained linear inversion method to resolve the ill-posed inverse problem.

Function $I^*(Y)$ can be expressed approximately by a piece-wise linear function [8]:

$$I^*(Y)=\sum_{K=1}^{N} I^*_K * C_K(Y) \tag{5}$$

where

$$C_k\ (Y)=\begin{cases}(Y-Y_{k-1})/(Y_k-Y_{k-1}) & Y_{k-1}\le Y\le Y_k\\ (Y_{k+1}-Y)/(Y_{k+1}-Y_k) & Y_k\le Y\le Y_{k+1}\\ 0 & \text{elsewhere}\end{cases}$$

here N was the total number of the divided layers, and the coefficients I^*_K are the heights of $I^*(Y)$ at abscissa values Y_k using the absorption depth scale.

Substituting Eq. (5) into Eq. (4) for each measured data point $[\sigma_i, I^*_{obs}(\sigma_i)]$ at each fixed θ, where $i=1,2,\ldots\ldots M$ and M is the total number of the measured patterns with different incident angle α, the final result will be:

$$[C]\{a\}=\{b\} \tag{6}$$

where

$$C_{ik}=\int C_k(Y)\exp(-\sigma_i Y)dY$$

$a_k=I^*_k$ and $b_i=I^*_{obs}(\sigma_i)$

The solution of Eq. (6) can be obtained by the constrained linear inversion method as follows:

$$\{a\}=(C^TC+\xi H^TH)^{-1}C^T\{b\} \tag{7}$$

where ξ represents the relative weight of the linear constraint term and H is:

$$H=\begin{bmatrix}-1 & 1 & 0 & \cdots & \cdots & 0\\ 0 & -1 & 1 & 0 & \cdots & 0\\ \cdot & \cdots & \cdots & \cdots & \cdots & \cdot\\ 0 & \cdots & 0 & -1 & 1 & 0\\ 0 & \cdots & \cdots & 0 & -1 & 1\end{bmatrix}_{(N-1\times N)}$$

Concerning the diffraction ability $I^*(Y)$ is non-negative, in Eq. (6) the solution $\{a\}$ should subject to this constraint. Thus, the NNLS algorithm was logically employed into the resolution process here.

Problem NNLS was defined as: Solve $A\boldsymbol{x}=\boldsymbol{b}$ to $\boldsymbol{x}\ge 0$. Where A is a given $m\times n$ matrix and $\boldsymbol{b}$ is a given m-vector. According to the algorithm from Bolle et al. [11], the resolving progress converges after a finite number of iterations. As to the Eq. (6), the matrix A, the vector $\boldsymbol{x}$ and $\boldsymbol{b}$ are corresponding to $[C]$, $\{a\}$ and $\{b\}$, respectively. Thus, by the combination of the two algorithms, the resulting $I^*(Y)$ can be calculated.

3. Experimental

The substrate of the sample was $SiO_2/Si(100)$. A SiO_2 layer of approximately 8000 Å was deposited on the Si substrate which functioned as the barrier to prevent a reaction between Si and Ni/Pd thin films. The bilayer film was prepared by a physical vapor deposition (PVD) method at a base vacuum level of 3×10^{-5} Pa. The Ni layer was on top of the Pd layer. The thickness of Pd and Ni layers were 750 and 1500 Å, respectively. The thermal annealing process took place in a vacuum-annealing furnace at a temperature 380°C for a 30-min duration. Cooling was achieved by laying the sample in the vacuum tunnel at the room temperature. A standard Al_2O_3 ultra-fine powder sample was used to obtain the factor $A(\alpha,\theta,\vec{s})$ in Eq. (1).

To improve the precision of the measured data, the experiments were performed on the Bruker D8 Discover diffractometer, sample holder equipped with a Gobel mirror and a 1/4 Eulerion cradle. With the application of Gobel mirror, the incident X-ray beam was highly parallel. The divergent angle of X-ray beam was approximately 0.04°. As shown in Fig. 2, the sample was able to rotate around three axes including: the normal to the surface of the sample; the axis perpendicular to the

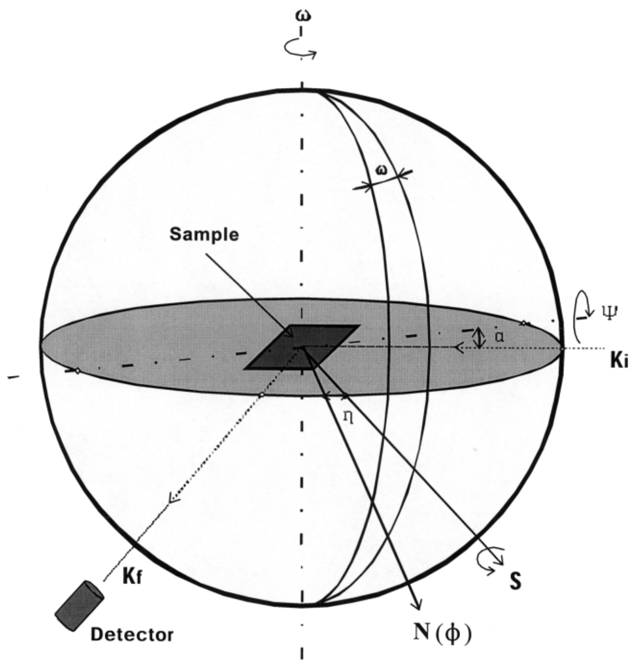

Fig. 2. The diffraction geometry of the Bruker D8 Discover diffractometer.

plane defined by K_i and K_f; and the horizontal axis formed by the sample surface intersecting with the plane defined by K_i and K_f. These correspond to rotation angles φ, ω, ψ, respectively, and for spherical geometry, so there are:

$$\begin{cases} ctg\,\varpi = [\cos\eta/\sin\alpha - \sin(\eta+\alpha_0)]/\cos(\eta+\alpha_0) \\ \cos\varphi = \sin(\eta-\varpi+\alpha_0)/\sin\eta \\ \cos\psi = \cos\eta/\cos(\eta-\varpi+\alpha_0) \end{cases} \tag{8}$$

where η is the angle between the axes s and n; α_0 is the original incident angle when the plane defined by K_i and K_f is perpendicular to the sample surface. Thus if the incident angle α is designated, the corresponding rotation angles φ, ω and ψ can be calculated, respectively, according to Eq. (8), ensuring the proposed method can be carried out on the D8 Discover diffractometer.

The measurements were carried out with asymmetric Bragg diffraction scheme shown in Fig. 1. The angle α_0 in Eq. (8) is 0.8°. The other 10 incident angles were from 1.0 to 19°, $M = 11$. It was also assumed that the annealed sample was divided into 11 analyzing sub-thin layers in absorption depth scale, $N = 11$.

The RBS experiments were carried out in a standard scattering configuration with the incidence of 3.023-MeV He^+ ions. The backscattering angle was 165° and the ion beam spot size was 1.0×1.0 mm^2.

4. Results

Fig. 3 showed the diffraction patterns of the sample by the conventional θ/2θ scanning. It should be noticed that a 'new' peak at approximately 42.56° could be observed in the annealed sample, which didn't corresponded to phases in the Ni/Pd binary phase diagram as shown in Fig. 4. This 'new' diffraction peak had also been observed by Lin and Spruiell in 1971, who reported a possible miscibility gap or long- or short-range ordering at low temperatures in the Ni–Pd binary phase diagram [12]. There are four diffraction peaks in the XRD pattern of the annealed sample as shown in Fig. 3. Rigidly, those diffraction peaks, except pure Pd diffraction peak at 40.15°, that correspond to solid solutions (S.S.) with different lattice parameters cannot be considered as the pure Pd or pure Ni diffraction peaks. For the aim of convenience, the 'Pd' peak, 'Solution' peak and 'Ni' peak are used here to label the peaks from the low angle to the high angle, respectively. The corresponding solid solutions were named as: 'Pd' S.S.; 'Solution' S.S.; and 'Ni' S.S.

The original experimental X-ray diffraction patterns are shown in Fig. 5, which were carried out using asymmetric diffraction geometry. With increasing incident angle, the X-ray penetrated deeper in the sample and the information from the deeper sub-layers further contributed to the measured XRD diffraction patterns. It was shown that with the increasing incidence angles, the relative integrated intensity of 'Pd' and 'Solution' peaks increased while that of the 'Ni' peak decreased. Each experimental XRD pattern is the sum of the diffraction information of all the sub-thin layers including the influence of absorption. From these patterns, the average and qualitative information along the depth can

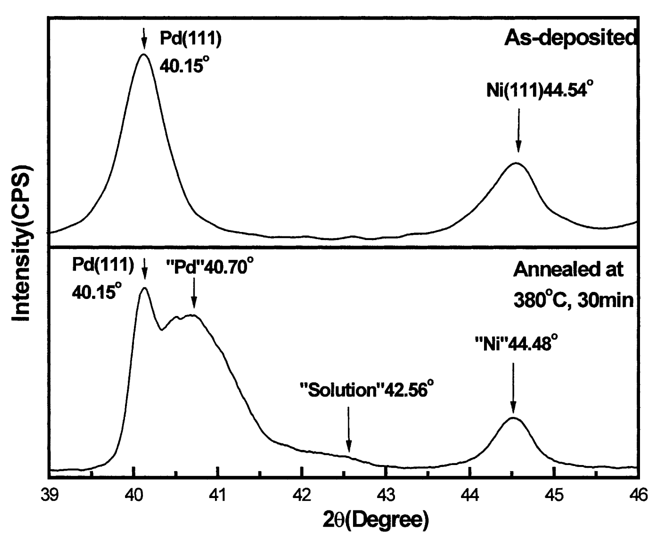

Fig. 3. Conventional XRD patterns of Ni/Pd films.

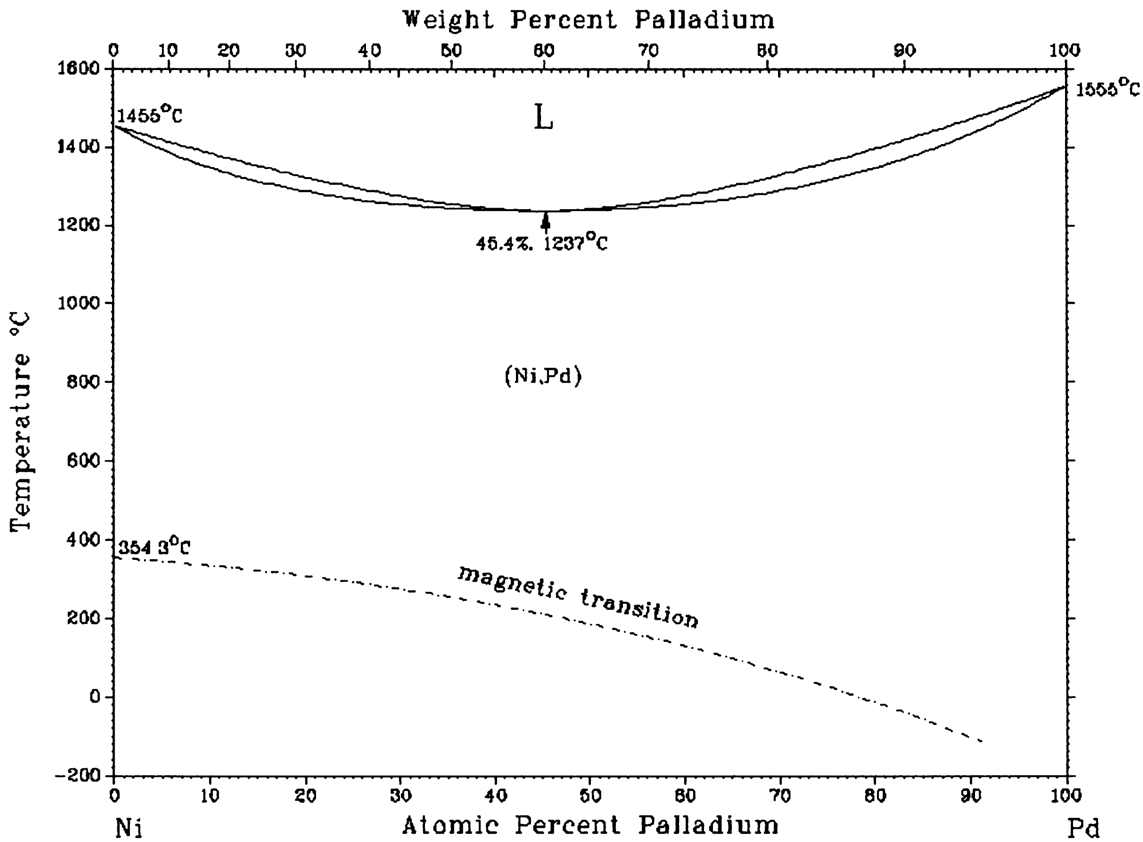

Fig. 4. The binary phase diagram of Pd/Ni (from the ASM's Binary Alloy Phase Diagrams, Second Edition).

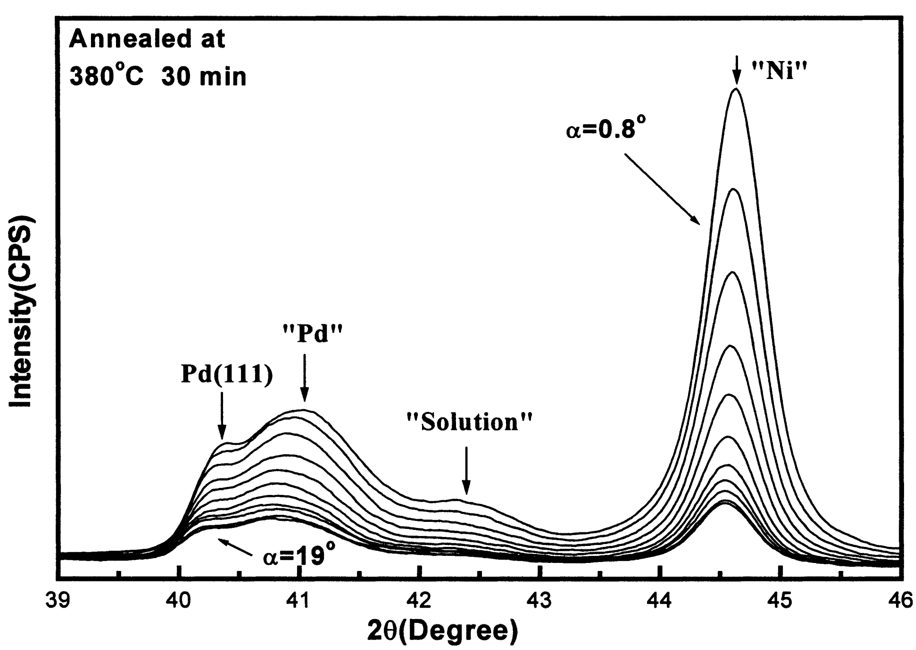

Fig. 5. The XRD experimental patterns of the Ni/Pd sample annealed at 380°C for 30 min. The incident angle α increases from 0.8 to 19°.

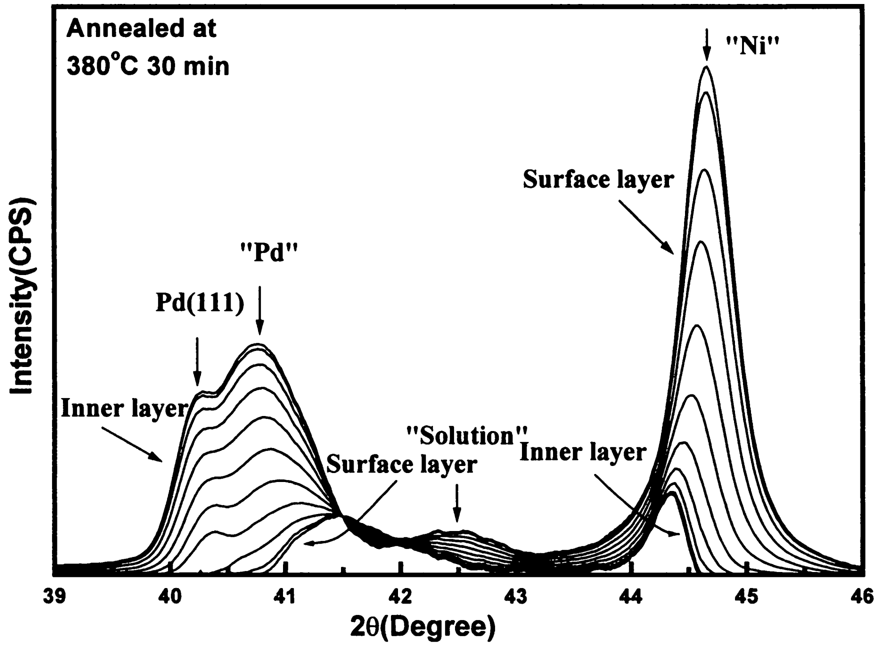

Fig. 6. The resolved XRD patterns of the Ni/Pd sample annealed at 380°C for 30 min. The M = N = 11 and D = 0.023.

be obtained, but the information concerning a certain sub-thin layer cannot be represented from them directly.

Fig. 6 shows the calculated patterns from the experimental diffraction patterns, which was deduced from the Eq. (6) with the mathematical algorithms described above. The resolved patterns, which are the XRD patterns corresponding to a sub-thin layer at different depths, are basically in accordance with the sample structures. In our work, the film was divided into 11 thin sub-layers. Since the total thickness was 225 nm, thus the thickness of each sub-layer was approximately 20 nm.

From the resolved XRD patterns, more quantitative and direct information about structure and phase at the certain depth can be accessed. In Fig. 6, it showed that the relative intensity of 'Ni' peak, which represented the 'Ni' S.S. containing more Ni, decreased monotonically with increasing depth. Moreover, the three S.S. peaks shifted to lower 2θ angles with the increase of the depth. The reason for the phenomenon was the lattice parameter of Pd was larger than that of Ni, and the concentration of element Pd increased from the surface to the Metal/SiO_2 interface. All these analytical results are consistent with Vegard's Law. The occurrence of the 'Solution' peak is of interest. The detailed analysis about the structure and the formation conditions of this solid solution is under investigation and will be discussed in a subsequent paper. It is clear that the peak intensities, peak positions and line profiles of the certain sub-layers can be separately resolved in the XRD patterns. The resolved patterns are useful to quantitatively analyze the interdiffusion and reaction mechanisms during the annealing process.

Based on the resolved patterns, the phase depth profile can be calculated according to the following procedure. For each calculated pattern, the integrated intensity for each diffraction peak was obtained after the peak overlap separation. Vegard's Law was used to calculate the concentrations of Ni and Pd in each phase or S.S from diffraction data. The structure factor F^2 for an FCC structure is 16 f^2 where f is the atomic scattering factor. In a disordered alloy or solid solution the average atomic scattering factor for the alloy is determined from

$$f_{av} = \sum_{a=1}^{a=n} (\mathrm{AtFrac}_a * f_a)$$

where f_{av} is the average atomic scattering factor of the alloy and AtFrac_a and f_a are the atomic fraction scattering factor of element, a in the alloy. Thus, according to the method mentioned above, the volume fraction of each phase can be determined. Then the phase depth profile can be calculated, as shown in Fig. 7.

It is clearly shown in Fig. 7 that in the surface layer of the sample the concentration of the 'Pd' S.S. was approximately 5 at.%. With the increasing depth, the concentration of 'Pd' S.S. increased, and at the depth of 220 nm the concentration was approximately 70 at.%. The lattice parameter of the solid solution did not vary significantly with depth. Ni and Pd both have FCC structures with lattice parameters of 3.523 and 3.867 Å, respectively. Considering the significant differences in lattice parameter and the lack of variation in the lattice parameter with depth would indicate that the composi-

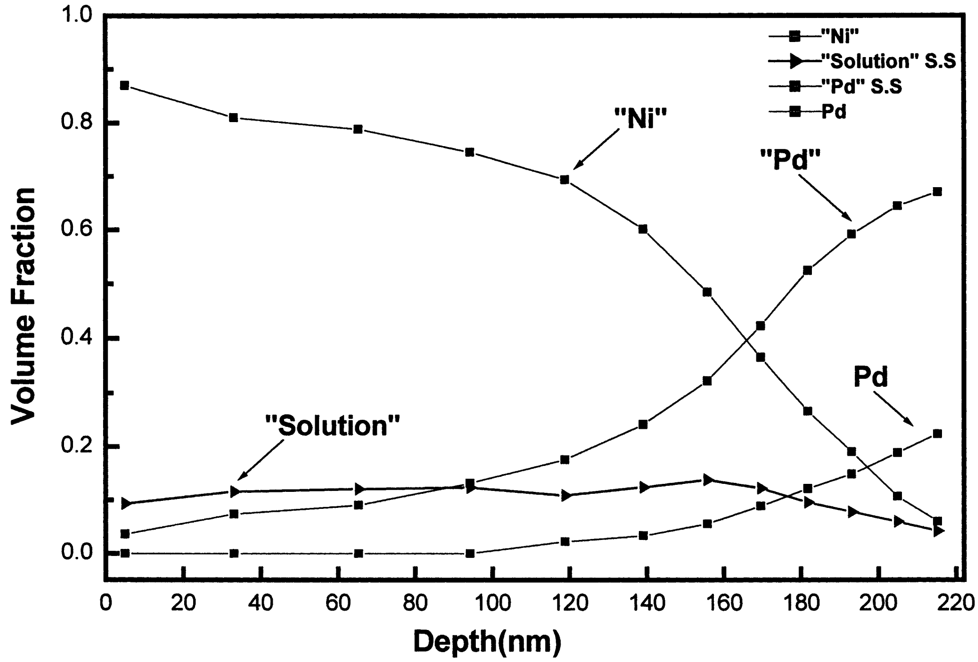

Fig. 7. The phase depth profile of the Ni/Pd sample annealed at 380°C for 30 min calculated from the resolved XRD patterns.

tion of the solid solution did not change significantly with depth. According to the phase depth profile, the depth was approximately 160 nm, where the elemental concentration of Ni was equal to that of Pd.

To compare the results, the element depth profiles of the sample were calculated from the RBS spectrum, as shown in Fig. 8. Comparing Fig. 7 and Fig. 8, the curve trends are similar. In the RBS element depth profile, the point of intersection of the two curves was approximately 160 nm, which was consistent with the result from the XRD phase depth profile. From the resolved patterns, the structure and phase information about the certain depth sub-thin layer can be achieved, however, only the element depth profile can be obtained from the RBS experimental spectrum.

5. Conclusions

In this paper, the CDP method was developed and

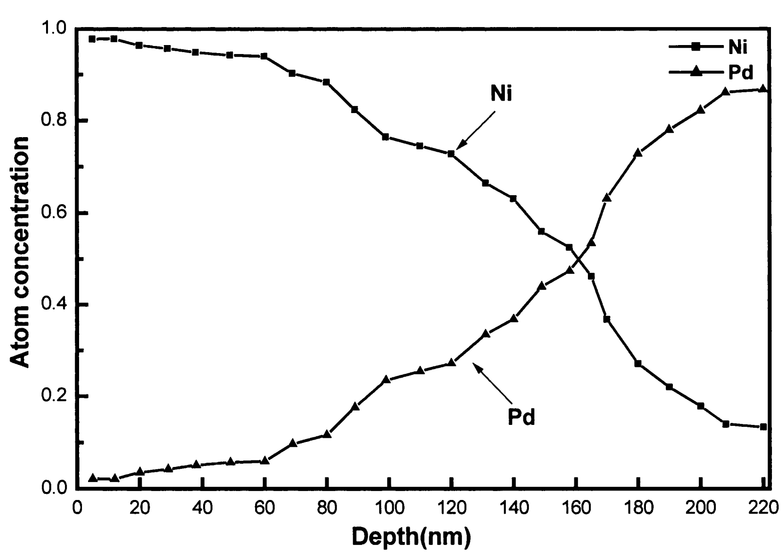

Fig. 8. The element depth profile of the Ni/Pd sample annealed at 380°C for 30 min calculated from the RBS spectrum.

applied to analyze annealed Ni/Pd samples. The operation of the Bruker D8 Discover diffractometer not only avoided the texture influence suitably, but also improved the data precision in the experiments. The NNLS method was first introduced into the resolving process, and the results approached the actual situation. The Ni/Pd sample, after thermal annealing containing four phases (solid solutions), was successfully resolved, which demonstrated that the CDP method worked well with the system including more than two phases. It is clear that by the present method the XRD patterns diffracted from layers at different depths can be extracted from the ordinary experimental patterns. Moreover, from the CDP method, the phase depth profile of the Ni/Pd sample was calculated, which was in agreement with the element depth profile from RBS analysis.

References

[1] Q.Z. Cong, D.Y. Yu, L.J. Wen, F.Q. Zhang, Thin Solid Films 213 (1992) 13.
[2] C. Qiuzi, J. Appl. Cryst. 25 (1992) 582.
[3] T.C. Huang, Adv. X-Ray Anal. 33 (1990) 91.
[4] M.F. Toney, T.C. Huang, S. Brennan, Z. Rek, J. Mater. Res. 3 (2) (1988) 351.
[5] A.V. Riessen, B.H. O'Connor, Adv. X-Ray Anal. 35 (1992) 169.
[6] J. Luo, K. Tao, Thin Solid Films 279 (1996) 53.
[7] K. Tao, J. Luo, Y. Xu, Vacu. Sci. Tech. (China) 15 (5) (1995) 326, In Chinese.
[8] B. Li, K. Tao, X. Liu, W. Miao, J. Luo, Thin Solid Films 353 (1999) 56.
[9] J. Luo, Y. Du, K. Tao, Powder Diffract. 11 (1996) 117.
[10] B. Bolle, A. Tidu, J.J. Heizmann, J. Appl. Cryst. 32 (1999) 27.
[11] C.L. Lawson, R.J. Hanson, Solving Least Squares Problem, Prentice–Hall, Inc., 1974, Chapter 23.
[12] W. Lin, J.E. Spruiell, Acta Metall. 19 (5) (1971) 451.